Semi-empirical metadynamics simulations for chemical glycosylation reactions

Kreupeling, B.M.; Hoogers, D.; Chen, S.; Meulenhoff, P.A.; Remmerswaal, W.A.; Codée, J.D.C.; Buda, F.

The Journal of Chemical Physics

RESEARCH ARTICLE | OCTOBER 13 2025

Semi-empirical metadynamics simulations for chemical glycosylation reactions

Special Collection: Michele Parrinello Festschrift

Bas Kreupeling ; Daan Hoogers ; Simon Chen; Pien A. Meulenhoff ; Wouter A. Remmerswaal ; Jeroen D. C. Codée ; Francesco Buda

J. Chem. Phys. 163, 144311 (2025)
https://doi.org/10.1063/5.0289569

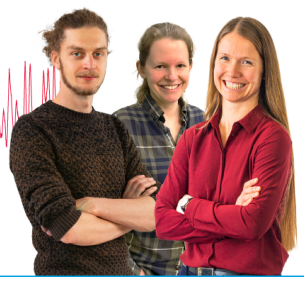

The Journal of Chemical Physics ARTICLE pubs.aip.org/aip/jcp

Semi-empirical metadynamics simulations for chemical glycosylation reactions

Cite as: J. Chem. Phys. 163, 144311 (2025); doi: 10.1063/5.0289569
Submitted: 8 July 2025 • Accepted: 22 September 2025 •
Published Online: 13 October 2025

Bas Kreupeling, Daan Hoogers, Simon Chen, Pien A. Meulenhoff, Wouter A. Remmerswaal,[a] Jeroen D. C. Codée,[b] and Francesco Buda[b]

AFFILIATIONS

Faculty of Science, Leiden Institute of Chemistry, Leiden University, Einsteinweg 55, 2333 CC Leiden, The Netherlands

Note: This paper is part of the JCP Special Topic, Michele Parrinello Festschrift.
[a]**Present address:** Center of Excellence for the Chemical Mechanisms of Life, Department of Chemistry—BMC, Uppsala University, 751 23 Uppsala, Sweden. wouter.remmerswaal@kemi.uu.se
[b]**Authors to whom correspondence should be addressed:** jcodee@chem.leidenuniv.nl and f.buda@lic.leidenuniv.nl

ABSTRACT

Glycosylation, the formation of glycosidic bonds, is a central yet challenging step in the chemical synthesis of complex carbohydrates due to its intricate regio- and stereochemical control. This study explores explicitly solvated, semi-empirical molecular dynamics (MD) simulations combined with multiple walker well-tempered metadynamics to investigate the mechanistic landscape of glycosylation involving a constrained glucose donor and a series of simple alcohol nucleophiles varying in nucleophilicity: ethanol, 2-monofluoroethanol, 2,2-difluoroethanol, and 2,2,2-trifluoroethanol. Our simulations reveal several mechanistic pathways depending on the nucleophile and substitution site. Stronger nucleophiles favor concerted S_N2 displacement, while weaker nucleophiles increasingly promote dissociative S_N1-like mechanisms and frontside attack pathways. This study demonstrates how semi-empirical MD simulations, combined with explicit solvation, can provide insights to understand the glycosylation reaction pathways.

I. INTRODUCTION

Carbohydrates are essential biomolecules involved in cellular signaling, immune recognition, metabolism, and structural organization.[1] Their functional diversity arises from extensive branching, varied glycosidic linkages, and stereochemical complexity,[2] which together present significant challenges for chemical synthesis. A key bottleneck is the glycosylation reaction—the formation of a glycosidic bond between an electrophilic donor sugar and a nucleophilic acceptor.[3] Achieving high levels of stereoselectivity in these reactions remains notoriously difficult, as the outcome is governed by subtle interactions among the donor structure, leaving group, protecting groups, solvent, additives, and the acceptor's nucleophilicity and steric profile.[4–7]

In a typical glycosylation reaction, a suitably protected glycosyl donor bearing an anomeric leaving group, reacts with a nucleophilic carbohydrate acceptor. The process begins with activation of the donor [Fig. 1 (i)] with a suitable activator to generate a mixture of reactive species. Most commonly, electrophilic activators are employed involving trifluoromethanesulfonate (triflate) counterions. The reactive intermediates that are formed include covalent intermediates [the α- and β-glycosyl triflates, Fig. 1 (iii_α) and (iii_β)] and non-covalent ion pairs [Fig. 1 (ii)]. These species then react with the acceptor through mechanisms that span the S_N1–S_N2 continuum [Fig. 1 (iv_α) and (iv_β)].[8–12] The anomeric triflates can be in rapid equilibrium by a triflate mediated interconversion pathway (see Fig. 1).[13–16]

Substitution reactions are a class of chemical transformations where a leaving group is replaced by a nucleophile.[17] The classical bimolecular substitution (S_N2) proceeds through a single concerted step in which nucleophilic attack and leaving-group departure occur simultaneously. This leads to inversion of stereochemistry at the carbon atom that is undergoing the substitution reaction. In contrast, the unimolecular substitution (S_N1) proceeds stepwise, with leaving-group departure forming a discrete carbocation intermediate that is subsequently attacked by the nucleophile.[18] This process can lead to

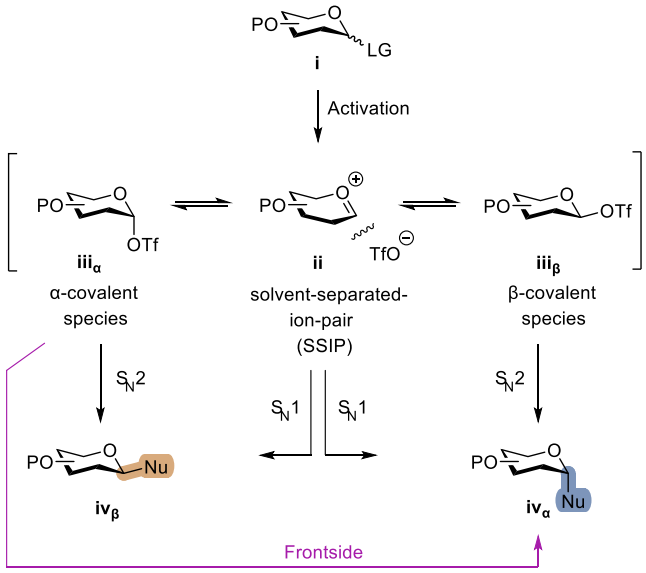

FIG. 1. Overview of the glycosylation reaction mechanism and its intermediates on the S_N1–S_N2 continuum. A generic protection group attached to a carbohydrate oxygen atom is indicated with "P," while "LG" indicates a generic leaving group. Moreover, "OTf" indicates the triflate group, and "Nu" indicates a generic nucleophile.

stereochemical mixtures. Real systems, however, often deviate from these idealized limits. A loose S_N2 describes an S_N2 pathway in which the transition state is more diffuse and/or asynchronous, reflecting an imbalance between bond formation and bond cleavage. An S_N2-like process departs from the ideal S_N2-scenario, by exhibiting a distorted geometry, partial stepwise character, or other intermediate features. Overall, the substitution occurs with inversion of stereochemistry. Similarly, an S_N1-like pathway shares significant features of an S_N1-reaction but without full development of the carbocation intermediate. Nonetheless, significant positive charge builds up at the carbon under substitution. Finally, a frontside S_N2 (S_N2-f) represents a concerted pathway in which nucleophilic attack and leaving group departure occur simultaneously, but the nucleophile attacks from the same side as the leaving group. In the context of enzymatic glycosylation reaction, this latter mechanism is often referred to as an S_Ni-mechanism.[19,20] The precise mechanism depends on the structure and reactivity of the donor, the counterion, solvent, temperature, concentration, and the nucleophilicity of the acceptor.

Computational studies have become an essential part of modern efforts to understand the detailed mechanisms of glycosylation. In particular, static density functional theory (DFT) approaches have been extensively applied to investigate reaction profiles, explore transition states, and examine the electronic features that drive selectivity.[9,15,16,18,21–32]

Static DFT calculations typically employ continuum solvation models, which, while efficient, may not fully account for situations in which specific solvent–solute interactions are critical. Limitations can arise in cases involving ion-pair collapse, hydrogen bonding, or solvent stabilization of charged intermediates. Introducing a few explicit solvent molecules may more accurately represent reaction conditions,[22,31] but this approach is dependent on chemical intuition and introduces a configurational bias. In some instances, locating transition states proves difficult, or reactant and product complexes may appear unstable under static conditions.[33]

Explicitly solvated molecular dynamics simulations address many of these limitations. By treating the solvent environment dynamically, these simulations naturally incorporate thermal fluctuations, hydrogen bonding, and solvent reorganization effects. Enhanced sampling methods, such as metadynamics,[34] further enable the exploration of complex free energy landscapes without requiring prior transition state guesses. These methods offer a more nuanced and realistic view of reaction mechanisms, especially in cases where solvation plays an active role.[35–37]

While *ab initio* molecular dynamics (AIMD), particularly Born–Oppenheimer molecular dynamics (MD) based on DFT, offers high accuracy,[37] its computational cost remains a major obstacle for exploratory mechanistic studies, especially when long timescales or large solvation shells are involved. Semi-empirical methods have previously been applied in the context of glycosylation chemistry,[35,36] illustrating their utility for capturing mechanistic features at a reduced cost. We here describe the use of the semi-empirical GFN-xTB method to investigate different possible glycosylation reaction pathways.[38] This approach offers a good balance between computational efficiency and chemical realism, representing a valid alternative to DFT-based simulations that turned out to be too resource-intensive to be practical for our systems (see Secs. S1.1–S1.3). Although the method does not yield precise energetic predictions, GFN-xTB generates qualitatively accurate reaction trajectories and solvation behavior. In this study, we use it as a first exploratory step to uncover mechanistic pathways and generate hypotheses for further validation.

Here, we have applied explicitly solvated metadynamics simulations to a well-defined glycosylation system involving a conformationally constrained glucosyl triflate. The relatively rigid ring conformation prevents large conformational changes of the donor glycoside six membered ring, enabling a consistent comparison across simulations. As acceptors, we selected four ethanol derivatives—ethanol (EtOH), 2-monofluoroethanol (MFE), 2,2-difluoroethanol (DFE), and 2,2,2-trifluoroethanol (TFE)—which systematically decrease in nucleophilicity. This set of model acceptors has been introduced to experimentally investigate the impact of acceptor nucleophilicity on glycosylation stereoselectivity.[39] van der Vorm *et al.* found that in the glycosylation reactions of a benzylidene protected glucosyl donor highly nucleophilic acceptors yield predominantly β-products, while weaker nucleophiles increasingly favor α-products.[10,39,40] This trend was proposed to reflect a shift in mechanism along the S_N1–S_N2 continuum. To investigate the interactions that are at the basis of the changing stereoselectivity, we explored the free energy landscapes of the reactions and we identified preferred paths, employing multiple-walker well-tempered metadynamics, a robust enhanced sampling method capable of capturing rare events and transition regions.[34,41,42] While the GFN-xTB method cannot provide quantitatively accurate energy barriers, our results offer a detailed picture of the solvation-driven dynamics underlying the different reaction pathways—a key step toward designing more effective carbohydrate syntheses.

We examine not only α- and β-face attack mechanisms but also frontside pathways involving the prevalent axial triflate. Recent computational work has shown that this mechanism can be

competitive or even dominant for weaker (and thus more acidic) nucleophiles.[33] Our method can capture the preference of weaker alcohol nucleophiles to shift toward frontside S_N2 pathways due to increased hydrogen bonding between the incoming nucleophile and the leaving group.[34,41,42]

II. COMPUTATIONAL DETAILS AND MODEL SYSTEMS

We studied the α- and β-face attack of the 2,3-*O*-methyl-4,6-*O*-methylidene glucosyl triflate donors [see Fig. 2(a)] by a series of simple nucleophilic alcohol acceptors [see Fig. 2(b)]. To reduce computational cost, while preserving key steric and electronic features, the benzylidene acetal and benzyl ether protecting groups, which are commonly used in synthetic chemistry, were replaced with their "truncated" methylidene and methyl analogs, respectively. This change from benzyl to methyl protection groups does not significantly affect the stereochemical outcome experimentally, as detailed in Sec. III A. For each simulation, we include the glycosyl donor and a single alcohol acceptor explicitly solvated in 50 dichloromethane (DCM) molecules within a periodic cubic simulation box, as shown in Fig. 2(c). The box size ($18.12 \times 18.12 \times 18.12$ Å^3) was obtained from a DFT NPT simulation, detailed in the supplementary material (Sec. S2).

All MD simulations were carried out using the Quickstep module implemented in CP2K version 2023.1.[43,44] The forces and energies are calculated at the semi-empirical level with GFN-xTB.[38] We propagated the NVT dynamics with a 0.5 fs time step and at a temperature of −40 °C. The temperature was controlled using a global stochastic velocity rescaling thermostat with a time constant of 100 fs.[45] To investigate the reaction mechanisms, we employed multiple-walker well-tempered metadynamics using PLUMED version 2.8.0.[46] Eight independent walkers were initialized from distinct reactant configurations to improve conformational sampling and avoid kinetic trapping. The metadynamics bias was applied along two collective variables (CVs), both based on smooth coordination numbers, which describe how close two atoms are in a continuous and differentiable way. Coordination numbers are a straightforward choice to describe a reaction when there are multiple atoms that can form covalent bonds, such as the bond formation and breaking with the triflate leaving group. The general form of the coordination number between two atoms C_{AB} is

$$C_{\mathrm{AB}} = \frac{1 - \left(\frac{r_{\mathrm{AB}}}{r_{\mathrm{AB},0}}\right)^n}{1 - \left(\frac{r_{\mathrm{AB}}}{r_{\mathrm{AB},0}}\right)^m}, \tag{1}$$

where r_{AB} is the instantaneous distance between atoms A and B, $r_{AB,0}$ can be interpreted as the distance after which the atoms are not coordinated anymore, and n and m are parameters that determine the smoothness of the transition. One CV (CN C^1–O^{Nu}) tracks the formation of the glycosidic bond by measuring the coordination between the anomeric carbon (C^1) and the nucleophilic oxygen of the acceptor (O^{Nu}). The second CV (CN C^1–O^{LG}) monitors the cleavage of the bond to the leaving group, which is a triflate anion in this case. Since the triflate leaving group contains three equivalent oxygen atoms, the coordination number of the triflate with C^1 (CN C^1–O^{LG}) was calculated as the smooth maximum using LogSumExp of the three individual coordination numbers with

$$\mathrm{CN}\ \mathrm{C}^1 - \mathrm{O}^{\mathrm{LG}} = \beta\left[\ln \sum_{i \in \mathrm{O}^{\mathrm{LG}}} \exp\left(\frac{C_{\mathrm{LG},i}}{\beta}\right)\right]^{-1}, \tag{2}$$

where $C_{LG,i}$ is the coordination number between C^1 and the ith oxygen atom of the leaving group, and β is a smoothing parameter that controls how sharply the soft maximum approaches the true maximum. To drive the reaction, we applied a well-tempered metadynamics bias potential along both CVs. Individual Gaussians were deposited every 100 fs, with a height of 0.1 kcal mol^{-1} and a width of 0.075. The chosen deposition time of 100 fs reflects a compromise between ensuring sufficient accuracy in free energy reconstruction and observing quasi-ergodic sampling within feasible simulation timescales. Notably, previous studies on glycosylation have employed shorter deposition times between 25 and 50 fs.[35–37,47] The bias factor γ was set to 60, which modulates the effective temperature in CV space, allowing efficient exploration of high-energy

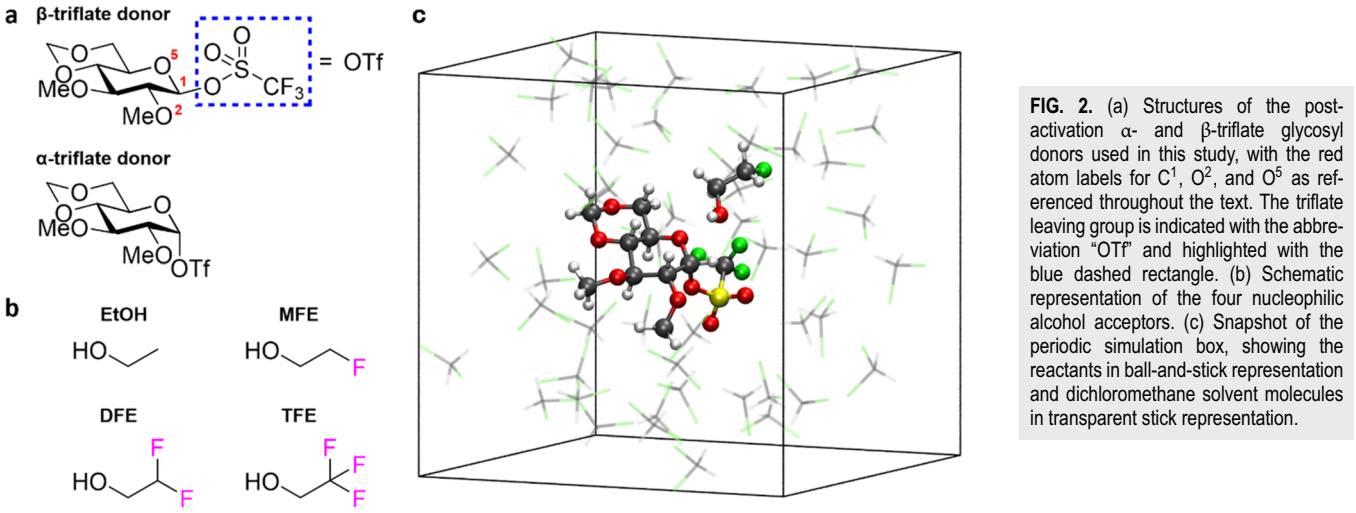

FIG. 2. (a) Structures of the post-activation α- and β-triflate glycosyl donors used in this study, with the red atom labels for C^1, O^2, and O^5 as referenced throughout the text. The triflate leaving group is indicated with the abbreviation "OTf" and highlighted with the blue dashed rectangle. (b) Schematic representation of the four nucleophilic alcohol acceptors. (c) Snapshot of the periodic simulation box, showing the reactants in ball-and-stick representation and dichloromethane solvent molecules in transparent stick representation.

configurations while preserving the underlying free energy surface (FES).

Although GFN-xTB enables us to run extensive trajectories at relatively low computational cost, it has some limitations. Because this semi-empirical method is not explicitly trained on transition-state-like geometries, its energetic predictions in the vicinity of the transition state may be unreliable. While the overall reaction trajectories are generally reasonable, the biasing potential in metadynamics can sometimes promote side reactions that would not occur in a DFT-based simulation. To mitigate these issues and maintain realistic chemical behavior, we applied a set of geometric restraints during the dynamics to prevent unlikely or unphysical transformations. Details on the exact form and implementation of these restraints are provided in the supplementary material (Sec. S3).

III. RESULTS

Building on our experimental findings that nucleophilicity of alcohol acceptors can affect the stereochemical outcome of glycosylation reactions of 4,6-*O*-benzylidene-protected glucose donors,[39,40] we sought to explore the origin of this trend using explicit-solvent metadynamics simulations. We first describe the characteristic features of the different mechanistic pathways using MFE as a representative acceptor, followed by a comparison of computed activation barriers across all nucleophiles.

A. Computational model validation

As described above, to reduce computational cost, our simulations employ glucose donors protected with a methylidene acetal and methyl ethers rather than the more sterically bulky benzylidene and benzyl groups. To establish that these changes do not significantly affect stereoselectivity of the reactions, we experimentally performed the chemical glycosylation reactions and compared the resulting α:β stereoselectivities with previously reported experimental results obtained using the benzylidene/benzyl-protected donors.[15] As shown in Table I, the stereoselectivity trends across the range of nucleophiles are consistent between the two donors, with only minor differences observed. This supports the use of methylidene groups in simulations as a chemically valid and computationally efficient alternative to benzylidene groups.

B. Backside attack on the β-triflate

Figure 3 shows the FES for the backside attack on the β-triflate with MFE. The energy surface shows a relatively shallow transition state zone. A lowest energy path can be found following a concerted S_N2-like mechanism. A saddle point is present in the TS region, at donor–acceptor and donor–leaving group bond distances of around 2.3 Å (see Table III). While the nucleophile approaches the anomeric center from the backside, the hydroxyl hydrogen is oriented toward the O^2 atom of the donor, forming a stabilizing hydrogen bond in the transition state (TS). This interaction facilitates the in-line displacement of the triflate leaving group, which can depart from the glucose donor adopting a distorted twist-boat conformation. In the TS region [Fig. 3(c)], the proton forms a hydrogen bond between the nucleophile oxygen and O^2 of the donor (H^{Nu}–O^2 = 2.13 Å; H^{Nu}–O^{Nu} = 0.97 Å). As the reaction proceeds [Fig. 3(d)], the proton is transferred further toward O^2 (H^{Nu}–O^2 = 1.04 Å; H^{Nu}–O^{Nu} = 1.45 Å). At later stages, not shown in the snapshots of Fig. 3, the proton is ultimately accepted by the leaving group.

In addition to this lowest energy concerted pathway, a pathway can also be observed in a region where both the nucleophile and leaving group are partially dissociated from the donor that is slightly

TABLE I. Model glycosylation reaction results comparing 2,3-*O*-methyl-4,6-*O*-methylidene (**1**) and 2,3-di-*O*-benzyl-4,6-*O*-benzylidene glucosyl donors (**2**). The stereoselectivity of the reaction is expressed as α:β and is based on ^{1}H-NMR of purified α/β-product mixtures. Pre-activation-based glycosylation conditions were used:[48] donor **1** or **2** (1 equiv), Tf_2O (1.3 equiv), Ph_2SO (1.3 equiv), TTBP (2.5 equiv), and DCM (0.05M), −80 to −60 °C, then add nucleophile (2 equiv) at −80 °C and allow to warm to −40 °C. [a] Glycosylation results for donor **2** were generated by Remmerswaal *et al.*[15]

		 A	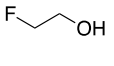 B	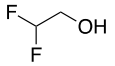 C	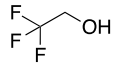 D
	Donor	**Product** α:β (yield)	**Product** α:β (yield)	**Product** α:β (yield)	**Product** α:β (yield)
1	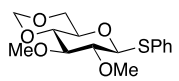	**1A** 27:73 (95%)	**1B** 46:54 (97%)	**1C** 80:20 (89%)	**1D** 97:3 (90%)
2	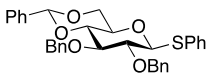	**2A**[a] 30:70 (80%)	**2B**[a] 50:50 (65%)	**2C**[a] 82:18 (95%)	**2D**[a] >98:2 (74%)

>90:10	>75:25	>60:40	50:50	<40:60	<25:75	<10:90

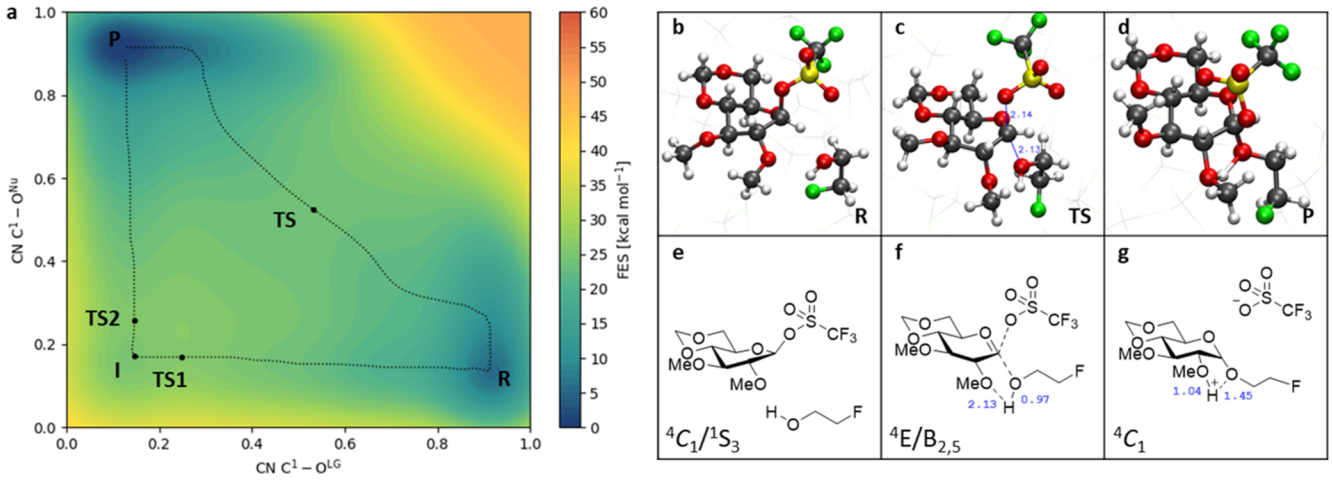

FIG. 3. Two-dimensional free energy surface (FES) for the glycosylation reaction via backside substitution of the β-triflate with monofluoroethanol (MFE), plotted as a function of donor–acceptor and donor–leaving group coordination numbers (a). The two minimum free energy paths are indicated by dotted black lines. Panels (b)–(d) show representative structures extracted along the S_N2-like reaction pathway, corresponding to the reactant (R), transition state (TS), and product (P) regions indicated on the FES. Panels (e)–(g) provide schematic representations of the same snapshots shown directly above, where we also report the carbohydrate conformation and relevant nucleophile hydrogen distances.

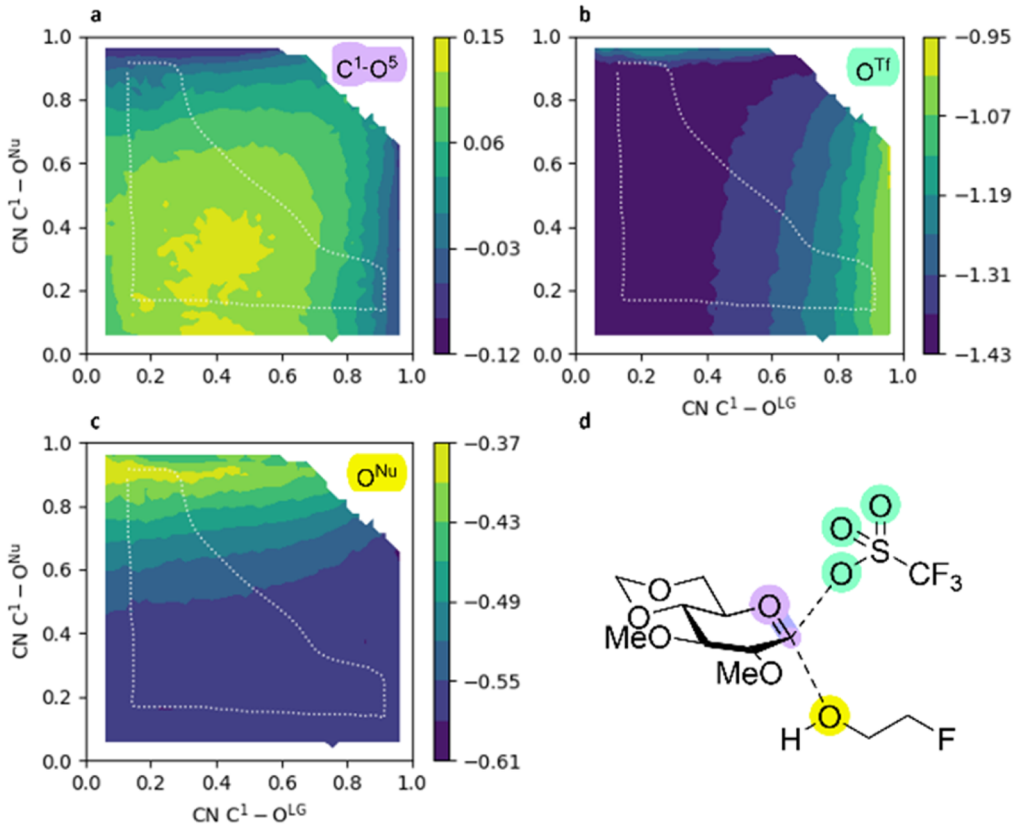

FIG. 4. Charge surfaces along the two coordination numbers for the backside attack on the β-triflate with MFE: (a) the anomeric carbon C^1 and ring oxygen O^5 of the donor, (b) the three oxygen atoms of the triflate leaving group, and (c) the nucleophilic oxygen of the acceptor. The minimum free energy paths are overlaid in white dotted lines in all panels. Panel (d) shows a representation of the donor–acceptor complex with the three atom groups highlighted in their respective colors, corresponding to panels (a)–(c).

higher in energy. This pathway represents a somewhat less favorable S_N1-like pathway involving a transient ion-pair, in which the glucose ring adopts a half chair conformation.

While this S_N1-like pathway is energetically less favorable for stronger nucleophiles such as EtOH and MFE, it becomes increasingly competitive for weaker nucleophiles such as DFE and TFE (see in the following and Sec. S4 of the supplementary material). This trend reflects the reduced ability of weak nucleophiles to stabilize the transition state of a concerted displacement, making a stepwise mechanism more accessible.

To analyze key charge rearrangements during glycosylation, we computed the conditional ensemble average of the Mulliken charges of a group of atoms A as a function of the collective variables $\boldsymbol{s} = \boldsymbol{\xi}(\boldsymbol{x})$. This defines a charge surface q_A, given by

$$q_A(\boldsymbol{s}) = \left\langle \prod_i \delta[\xi_i(\boldsymbol{x}) - s_i] \sum_{j \in A} q_j(\boldsymbol{x}) \right\rangle. \tag{3}$$

Here, q_j denotes the Mulliken charge of atom j, $\boldsymbol{x}$ is the atomic configuration, and δ is the Dirac delta function. The ensemble average $\langle \cdot \rangle$ is computed over all sampled configurations in the metadynamics trajectories. The charge surfaces are calculated along the same collective variables that were biased during the metadynamics trajectories. In practice, the delta function is approximated by finite-width bins, and the average is evaluated on a $[0,1] \times [0,1]$ regular grid with a grid spacing of 0.02. This approach allows us to resolve how charge distribution evolves across the reaction landscape and to correlate changes in electronic structure with specific chemical features.

In Fig. 4(a), the charges on the anomeric carbon C^1 and the ring oxygen O^5 of the donor increase as the system approaches the transition state, consistent with the buildup of oxocarbenium ion character. This charge accumulation then dissipates upon product formation. Figure 4(b) shows that the triflate oxygen atoms become increasingly negative as the donor-leaving group bond breaks, reflecting electron density accumulation on the departing group. Conversely, the nucleophilic oxygen of the alcohol acceptor [Fig. 4(c)] becomes more positively charged as it forms a covalent bond with C^1, indicating donation of electron density into the developing glycosidic bond. Together, these charge surfaces indicate that GFN-xTB captures the expected electronic features of glycosylation chemistry.

C. Backside attack on the α-triflate

The computed FES for the backside substitution on the α-triflate shows two mechanistically distinct pathways: a loose S_N2 mechanism and a stepwise S_N1 pathway. The GFN-xTB method provides slightly lower activation barriers for the S_N1 route. This is consistent for all studied nucleophiles, but stands at odds with the mechanistic picture drawn up based on the experimental results.[39]

In the loose S_N2 pathway, bond formation and bond breaking occur asynchronously. The donor ring adopts a slightly distorted chair conformation, and the transition state features elongated bond distances between both the nucleophile and the anomeric carbon, and the anomeric carbon and the leaving group. These geometries reflect partial charge development and a loss of concerted character. Figures 5(b)–5(d) show representative snapshots of the reactant, transition state, and product along this reaction path. The reaction begins with a nucleophilic approach and donor deformation, followed by partial departure of the leaving group and bond formation with the nucleophile.

The S_N1 pathway involves nearly complete cleavage of the C^1–O^{Tf} bond prior to nucleophilic attack. This results in the formation of a discrete, charge-separated oxocarbenium ion-triflate anion pair intermediate. The reaction then proceeds through a second transition state where the nucleophile approaches and the bond to the anomeric carbon starts to form. In our simulation, the proton from MFE is simultaneously being transferred to the triflate anion

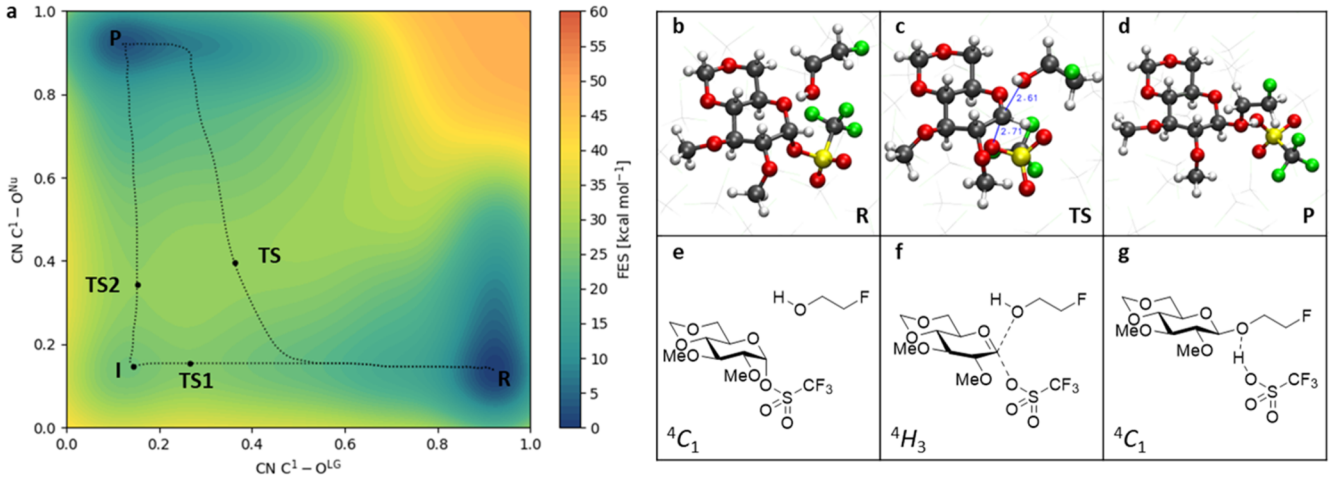

FIG. 5. Two-dimensional free energy surface for the glycosylation reaction via backside substitution of the α-triflate with monofluoroethanol (MFE), plotted as a function of donor–acceptor and donor–leaving group coordination numbers (a). The two minimum free energy paths are indicated by the dotted black lines. Panels (b)–(d) show representative structures extracted along the S_N2-like reaction pathway, corresponding to the reactant (R), transition state (TS), and product (P) regions indicated on the FES. Panels (e)–(g) provide schematic representations of the same snapshots shown directly above, where we also report the carbohydrate conformation.

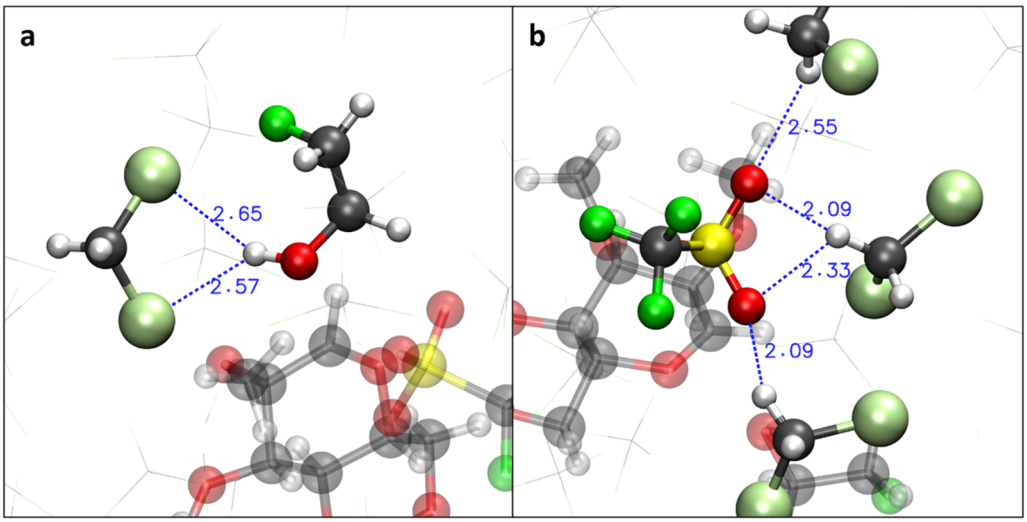

FIG. 6. Solvent–solute interactions in the transition state [as shown in Fig. 5(c)] of the backside α-triflate substitution pathway. (a) Solvent molecules orient their chlorine atoms toward the hydroxyl hydrogen atom of the nucleophilic acceptor. (b) The same configuration viewed from a different angle highlights how hydrogen atoms of DCM molecules point toward the oxygen atoms of the triflate leaving group. The blue dotted lines indicate key distances that reflect these specific interactions.

that has transposed to the side of the glucose ring to reach over to the acceptor proton. The ion pair intermediate was observed on the FES for all nucleophiles (see Sec. S4), as shown in Fig. 5(a) for MFE.

In the backside α-triflate S_N2 pathway, we observe pronounced solvent–solute interactions that contribute to stabilizing the transition state configurations (Fig. 6). In particular, the chlorine atoms of the DCM solvent molecules preferentially orient toward the hydroxyl hydrogen atom of the alcohol acceptor [Fig. 6(a)], while the hydrogen atoms of DCM align toward the negatively charged oxygen atoms of the triflate leaving group [Fig. 6(b)]. These directional interactions are clear signatures of electrostatic stabilization provided by the solvent, underscoring the importance of explicit solvation in capturing the electrostatic interactions during the reaction. Similarly, we observe such stabilizing solvent–solute interactions in the case of the S_N1 mechanism for the α-triflate substitution pathway (see supplementary material, S5).

D. Frontside attack on the α-triflate

Frontside substitution on the α-triflate was explored by applying angular restraints in our simulations. As shown in Fig. 7(a),

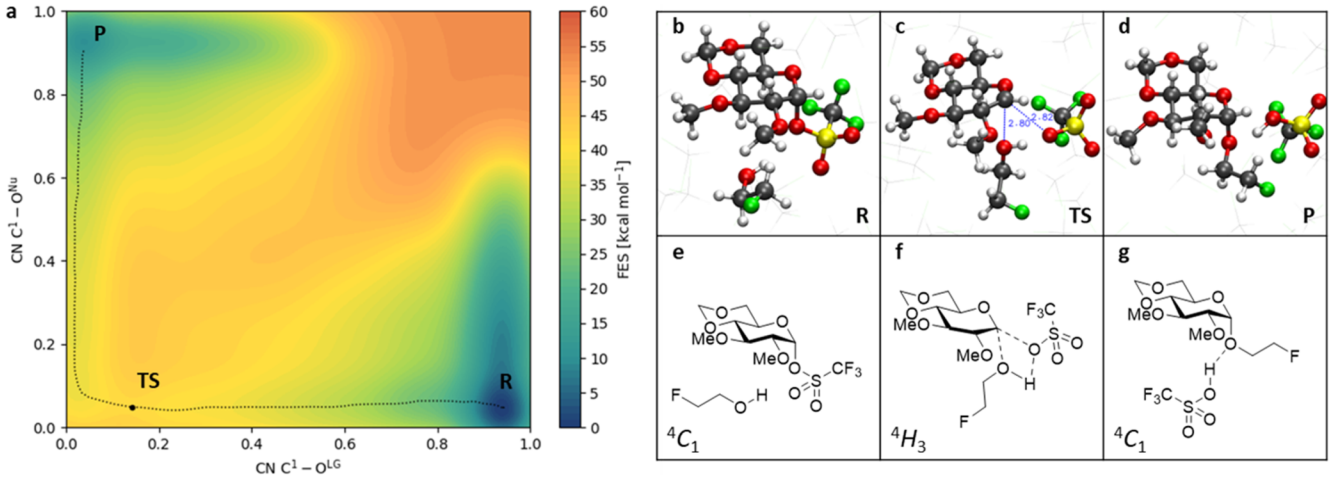

FIG. 7. Two-dimensional free energy surface for the glycosylation reaction via backside substitution of the α-triflate with monofluoroethanol (MFE), plotted as a function of donor–acceptor and donor–leaving group coordination numbers (a). The minimum free energy path (MFEP) is indicated by the dotted black line. Panels (b)–(d) show representative structures extracted along the reaction pathway, corresponding to the reactant (R), transition state (TS), and product (P) regions indicated on the FES. Panels (e)–(g) provide schematic representations of the same snapshots shown directly above, where we also report the carbohydrate conformation.

this mechanism proceeds via a rather dissociative, S_N1-like pathway. Representative snapshots of the reactant, transition state, and product structures [Figs. 7(b)–7(d)] illustrate the key stages along the reaction pathway. Initially, the nucleophile approaches the donor, which undergoes conformational deformation while the triflate leaving group begins to dissociate. Subsequently, the leaving group forms a complex with the acceptor, followed by a closer approach and bond formation between the nucleophile and the donor's anomeric carbon. Concurrently, a proton transfer occurs from the nucleophile to the leaving group, stabilizing the product complex.

E. Comparison across pathways and nucleophiles

The computed activation free energy barriers for all glycosylation reactions, summarized in Table II (see also the FES's in Sec. S4), reveal mechanistic trends of how the nucleophile identity and substitution pattern influence the different reaction paths.

The S_N2 barriers for the substitution of both the α-triflate and the β-triflate increase gradually in going from EtOH to TFE, consistent with the expected decrease in nucleophilicity across the alcohol series. This trend reflects the reduced capacity of more weakly basic acceptors to stabilize the transition state for in-line displacement. The transition state energy for the S_N1 pathways is affected less by the nature of the nucleophile. As a result, the S_N2 reactions become less favorable for the weaker nucleophiles. These trends support the notion that stronger nucleophiles promote S_N2 mechanisms, while weaker nucleophiles increase the feasibility of stepwise S_N1 pathways. Notably, across all pathways where S_N1-like intermediates were observed, the free energies of the intermediates on the S_N1 trajectories are very close to those of their adjacent transition states (typically within 1–2 kcal mol^{-1}). This proximity indicates that these intermediates are transient and unstable, functioning more as shallow wells along the reaction path than as kinetically relevant species.

The activation barriers for the frontside substitution on the α-triflate for EtOH and MFE are the highest among the possible pathways. For DFE and TFE, on the other hand, the barriers for frontside substitution are similar to the barriers of the other pathways, making this pathway competitive for the most acidic/least nucleophilic alcohols.

TABLE II. Computed activation free energies $\Delta F^{\ddagger}$ (referenced to the reactant state) for glycosylation reactions involving four alcohol nucleophiles (EtOH, MFE, DFE, and TFE) across three mechanistic pathways: backside attack on the β-triflate, backside attack on the α-triflate, and frontside attack on the α-triflate. Only the highest barrier along the MFEP of the backside S_N1 and frontside pathways are reported.

		$\Delta F^{\ddagger}$ (kcal mol^{-1})			
Reaction pathway	FES point	EtOH	MFE	DFE	TFE
Backside β-triflate	S_N2 TS	23.9	23.8	26.2	27.2
	S_N1 TS	27.6	26.4	27.4	27.7
Backside α-triflate	S_N2 TS	25.7	25.7	27.9	27.7
	S_N1 TS	25.9	25.0	26.7	27.4
Frontside α-triflate	TS	34.3	31.5	26.3	27.7

TABLE III. Donor–leaving group (d_{LG}) and donor–nucleophile (d_{Nu}) distances at the S_N2 transition states (TS) and S_N1-like intermediates (I) along the minimum free energy paths for each reaction pathway and nucleophile. Distances are reported for three mechanistic regimes: backside substitution on the β-triflate, backside substitution on the α-triflate, and frontside substitution on the α-triflate. The distances are obtained from the saddle points and minima along the minimum free energy path.

		Distances (Å)							
		EtOH		MFE		DFE		TFE	
Reaction pathway	FES point	d_{LG}	d_{Nu}	d_{LG}	d_{Nu}	d_{LG}	d_{Nu}	d_{LG}	d_{Nu}
Backside β-triflate	S_N2 TS	2.19	2.24	2.26	2.25	2.31	2.19	2.51	2.22
	S_N1 I	3.02	3.00	2.99	3.09	3.00	3.09	2.94	3.12
Backside α-triflate	S_N2 TS	2.38	2.34	2.47	2.53	2.54	2.54	2.69	2.55
	S_N1 I	2.99	3.07	3.08	3.09	3.05	3.05	2.97	3.06
Frontside α-triflate	S_N2 TS	3.37	2.95	3.78	3.10	...	...	...	...
	S_N1 I	...	...	...	...	3.54	3.64	3.42	3.53

The donor–acceptor and donor–leaving group bond distances at the transition states and S_N1-like intermediates are shown in Table III. For the backside substitution of both the α- and β-triflate, the C^1–O^{Nu} distance in the S_N2 transition state remains relatively constant across all alcohols, but the C^1–O^{LG} bond shows progressive elongation in the transition states going from EtOH to TFE. This trend reflects the increasing difficulty of bond cleavage with the less nucleophilic acceptors. In all S_N1-like intermediates, the donor–leaving group and donor–nucleophile distances are around 3.0–3.1 Å, indicative of a loose ion pair. This geometry is consistent with a dissociated intermediate where neither covalent bond is fully formed. Stabilization likely arises from electrostatic interactions with solvent.

In the transition states of the frontside substitution of the α-triflate, the C^1–O^{LG} distance and C^1–O^{Nu} distances are the largest of all pathways. The large distances likely reflect the geometric strain associated with a frontside approach and a highly dissociative mechanism. The high energy that is associated with the dissociation of the donor and leaving group can be compensated by the hydrogen bond that develops between the nucleophile and the leaving group.

IV. CONCLUSIONS AND DISCUSSION

Our simulations have illustrated the mechanistic landscape governing glycosylation reactions with a set of model alcohols. The simulations have shown very "shallow" landscapes with broad transition zones in which the S_N2 transition states are close in energy to the ones found in the alternative S_N1-like trajectories. The energy landscapes have indicated how variations in acceptor nucleophilicity influence the balance between concerted and dissociative mechanisms. The barrier for the backside S_N2 transition states become higher for the weaker nucleophiles, while those for the stepwise S_N1-like pathways show a less steep increase, rendering the S_N1-like pathways relatively more favorable for the weaker nucleophiles. The frontside substitution is unfavorable for the stronger nucleophiles, but becomes relatively more attractive for the more acidic acceptors. This may be accounted for by the more stabilizing hydrogen bond between the acceptor alcohol and the leaving group. In the backside substitution of the β-triflate, a stabilizing hydrogen bond is observed between O^2 of the donor and the incoming alcohol. In the substitution of the α-triflate, the hydrogen of the incoming alcohol is transferred to the triflate, which moves around the anomeric carbon. This study illustrates how explicitly solvated, semi-empirical molecular dynamics combined with enhanced sampling can uncover mechanistic details in glycosylation reactions that can remain obscured in more traditional static approaches.

While the current framework offers valuable qualitative insight into glycosylation mechanisms, the accuracy of the semiempirical GFN-xTB approach may not be enough to distinguish between reaction paths that are very close in their free energy barriers. A possible strategy to refine the free energy surfaces is by reweighting semi-empirical trajectories using higher-level quantum chemical methods via free energy perturbation.[49] In addition, replacing simple geometric CVs with machine learning CVs that can capture proton transfer, solvation effects, and other mechanistically relevant motions could further increase the accuracy of biased simulations.[50–53] The mechanistic understanding gained here also opens the door to building reactive machine learning potentials using active learning.[54–57] By focusing sampling on chemically relevant regions of configuration space, such potentials could retain key electronic features of glycosylation chemistry while enabling broader and more efficient exploration of donor–acceptor combinations and solvent effects.

SUPPLEMENTARY MATERIAL

The supplementary material provides additional computational details, validation tests, figures, and tables complementing and supporting the information in the manuscript.

ACKNOWLEDGMENTS

The simulations reported in this work were sponsored by the Nederlandse Organisatie voor Wetenschappelijk Onderzoek (NWO) – Domain Science for the use of supercomputer facilities (Grant No. 19689).

AUTHOR DECLARATIONS

Conflict of Interest

The authors have no conflicts to disclose.

Author Contributions

Bas Kreupeling: Conceptualization (equal); Data curation (equal); Formal analysis (equal); Investigation (equal); Methodology (equal); Resources (supporting); Supervision (equal); Validation (equal); Visualization (equal); Writing – original draft (lead); Writing – review & editing (equal). **Daan Hoogers**: Data curation (equal); Formal analysis (equal); Investigation (equal); Methodology (equal); Validation (equal); Visualization (equal); Writing – original draft (supporting); Writing – review & editing (equal). **Simon Chen**: Conceptualization (equal); Data curation (equal); Formal analysis (equal); Investigation (equal); Methodology (equal); Validation (equal); Visualization (equal); Writing – review & editing (equal). **Pien A. Meulenhoff**: Conceptualization (equal); Data curation (equal); Formal analysis (equal); Investigation (equal); Validation (equal); Visualization (equal); Writing – review & editing (equal). **Wouter A. Remmerswaal**: Conceptualization (equal); Data curation (equal); Formal analysis (equal); Investigation (equal); Methodology (equal); Validation (equal); Visualization (equal); Writing – review & editing (equal). **Jeroen D. C. Codée**: Conceptualization (equal); Data curation (equal); Formal analysis (equal); Funding acquisition (lead); Investigation (equal); Supervision (equal); Validation (equal); Visualization (equal); Writing – review & editing (equal). **Francesco Buda**: Conceptualization (equal); Data curation (equal); Formal analysis (equal); Funding acquisition (lead); Investigation (equal); Methodology (equal); Resources (lead); Supervision (equal); Validation (equal); Visualization (equal); Writing – review & editing (equal).

DATA AVAILABILITY

The data that support the findings of this study are available from the corresponding author upon reasonable request.

REFERENCES

[1] H.-J. Gabius, M. Cudic, T. Diercks, H. Kaltner, J. Kopitz, K. H. Mayo, P. V. Murphy, S. Oscarson, R. Roy, A. Schedlbauer, S. Toegel, and A. Romero, "What is the sugar code?," ChemBioChem **23**(13), e202100327 (2022).

[2] D. B. Werz, R. Ranzinger, S. Herget, A. Adibekian, C.-W. von der Lieth, and P. H. Seeberger, "Exploring the structural diversity of mammalian carbohydrates ('glycospace') by statistical databank analysis," ACS Chem. Biol. **2**(10), 685–691 (2007).

[3] S. S. Nigudkar and A. V. Demchenko, "Stereocontrolled 1,2-*cis* glycosylation as the driving force of progress in synthetic carbohydrate chemistry," Chem. Sci. **6**(5), 2687–2704 (2015).

[4] S. Chatterjee, S. Moon, F. Hentschel, K. Gilmore, and P. H. Seeberger, "An empirical understanding of the glycosylation reaction," J. Am. Chem. Soc. **140**(38), 11942–11953 (2018).

[5] T. Hansen, S. van der Vorm, C. Tugny, W. A. Remmerswaal, J. M. A. van Hengst, G. A. van der Marel, and J. D. C. Codée, "2.03—Stereoelectronic effects in glycosylation reactions," in *Comprehensive Glycoscience*, 2nd ed., edited by J. J. Barchi (Elsevier, Oxford, 2021), pp. 83–102.

[6] C.-W. Chang, M.-H. Lin, C.-H. Wu, T.-Y. Chiang, and C.-C. Wang, "Mapping mechanisms in glycosylation reactions with donor reactivity: Avoiding generation of side products," J. Org. Chem. **85**(24), 15945–15963 (2020).

[7] C.-W. Chang, M.-H. Lin, and C.-C. Wang, "Statistical analysis of glycosylation reactions," Chem.: Eur. J. **27**(8), 2556–2568 (2021).

[8] P. O. Adero, H. Amarasekara, P. Wen, L. Bohé, and D. Crich, "The experimental evidence in support of glycosylation mechanisms at the S_N1–S_N2 interface," Chem. Rev. **118**(17), 8242–8284 (2018).

[9] J. M. A. van Hengst, R. J. C. Hellemons, W. A. Remmerswaal, K. N. A. van de Vrande, T. Hansen, S. van der Vorm, H. S. Overkleeft, G. A. van der Marel, and J. D. C. Codée, "Mapping the effect of configuration and protecting group pattern on glycosyl acceptor reactivity," Chem. Sci. **14**(6), 1532–1542 (2023).

[10] S. van der Vorm, T. Hansen, J. M. A. van Hengst, H. S. Overkleeft, G. A. van der Marel, and J. D. C. Codée, "Acceptor reactivity in glycosylation reactions," Chem. Soc. Rev. **48**(17), 4688–4706 (2019).

[11] P. R. Andreana and D. Crich, "Guidelines for *O*-glycoside formation from first principles," ACS Cent. Sci. **7**(9), 1454–1462 (2021).

[12] M. Huang, P. Retailleau, L. Bohé, and D. Crich, "Cation clock permits distinction between the mechanisms of α- and β-*O*- and β-*C*-glycosylation in the mannopyranose series: Evidence for the existence of a mannopyranosyl oxocarbenium ion," J. Am. Chem. Soc. **134**(36), 14746–14749 (2012).

[13] P. H. Moons, F. F. J. de Kleijne, T. van Wieringen, F. ter Braak, H. R. Almizori, L. J. H. Jakobs, W. P. M. de Kleijne, F. P. J. T. Rutjes, J. Martens, J. Oomens, P. A. Korevaar, P. B. White, and T. J. Boltje, "Elucidating the Curtin–Hammett principle in glycosylation reactions: The decisive role of equatorial glycosyl triflates," J. Am. Chem. Soc. **147**(26), 22597–22608 (2025).

[14] F. F. J. de Kleijne, F. ter Braak, D. Piperoudis, P. H. Moons, S. J. Moons, H. Elferink, P. B. White, and T. J. Boltje, "Detection and characterization of rapidly equilibrating glycosylation reaction intermediates using exchange NMR," J. Am. Chem. Soc. **145**(48), 26190–26201 (2023).

[15] W. A. Remmerswaal, H. Elferink, K. J. Houthuijs, T. Hansen, F. ter Braak, G. Berden, S. van der Vorm, J. Martens, J. Oomens, G. A. van der Marel, T. J. Boltje, and J. D. C. Codée, "Anomeric triflates versus dioxanium ions: Different product-forming intermediates from 3-acyl benzylidene mannosyl and glucosyl donors," J. Org. Chem. **89**(3), 1618–1625 (2024).

[16] A. G. Santana, L. Montalvillo-Jiménez, L. Díaz-Casado, F. Corzana, P. Merino, F. J. Cañada, G. Jiménez-Osés, J. Jiménez-Barbero, A. M. Gómez, and J. L. Asensio, "Dissecting the essential role of anomeric β-triflates in glycosylation reactions," J. Am. Chem. Soc. **142**(28), 12501–12514 (2020).

[17] J. Clayden, N. Greeves, S. Warren, J. Clayden, N. Greeves, and S. Warren, *Organic Chemistry*, 2nd ed. (Oxford University Press, Oxford, NY, 2012).

[18] T. Hansen, L. Lebedel, W. A. Remmerswaal, S. van der Vorm, D. P. A. Wander, M. Somers, H. S. Overkleeft, D. V. Filippov, J. Désiré, A. Mingot, Y. Bleriot, G. A. van der Marel, S. Thibaudeau, and J. D. C. Codée, "Defining the S_N1 side of glycosylation reactions: Stereoselectivity of glycopyranosyl cations," ACS Cent. Sci. **5**(5), 781–788 (2019).

[19] R. D. Guthrie and W. P. Jencks, "IUPAC recommendations for the representation of reaction mechanisms," Acc. Chem. Res. **22**(10), 343–349 (1989).

[20] J. Chan, A. Tang, and A. J. Bennet, "A stepwise solvent-promoted S_Ni reaction of α-D-glucopyranosyl fluoride: Mechanistic implications for retaining glycosyltransferases," J. Am. Chem. Soc. **134**(2), 1212–1220 (2012).

[21] T. Hosoya, P. Kosma, and T. Rosenau, "Theoretical study on the effects of a 4,6-*O*-diacetal protecting group on the stability of ion pairs from D-mannopyranosyl and D-glucopyranosyl triflates," Carbohydr. Res. **411**, 64–69 (2015).

[22] T. Hosoya, T. Takano, P. Kosma, and T. Rosenau, "Theoretical foundation for the presence of oxacarbenium ions in chemical glycoside synthesis," J. Org. Chem. **79**(17), 7889–7894 (2014).

[23] H. Satoh, H. S. Hansen, S. Manabe, W. F. van Gunsteren, and P. H. Hünenberger, "Theoretical investigation of solvent effects on glycosylation reactions: Stereoselectivity controlled by preferential conformations of the intermediate oxacarbenium-counterion complex," J. Chem. Theory Comput. **6**(6), 1783–1797 (2010).

[24] A. Guo, Y. Xu, Z. Jia, T.-P. Loh, and X.-W. Liu, "Unraveling chemical glycosylation: DFT insights into factors imparting stereoselectivity," Green Synth. Catal. **6**(3), 302–310 (2025).

[25] T. Hansen, H. Elferink, J. M. A. van Hengst, K. J. Houthuijs, W. A. Remmerswaal, A. Kromm, G. Berden, S. van der Vorm, A. M. Rijs, H. S. Overkleeft, D. V. Filippov, F. P. J. T. Rutjes, G. A. van der Marel, J. Martens, J. Oomens, J. D. C. Codée, and T. J. Boltje, "Characterization of glycosyl dioxolenium ions and their role in glycosylation reactions," Nat. Commun. **11**(1), 2664 (2020).

[26] D. M. Whitfield, "Plausible transition states for glycosylation reactions," Carbohydr. Res. **356**, 180–190 (2012).

[27] K. M. Dorst, O. Engström, T. Angles d'Ortoli, H. Mobarak, A. Ebrahemi, U. Fagerberg, D. M. Whitfield, and G. Widmalm, "On the influence of solvent on the stereoselectivity of glycosylation reactions," Carbohydr. Res. **535**, 109010 (2024).

[28] M. Armand, A. Nin-Hill, A. Ardá, E. Berrino, J. Désiré, A. Martin-Mingot, B. Michelet, J. Jiménez-Barbero, Y. Blériot, C. Rovira, and S. Thibaudeau, "Glycosylium ions in superacid mimic the transition state of enzyme reactions," J. Am. Chem. Soc. **146**(47), 32618–32626 (2024).

[29] T. Nukada, A. Berces, M. Z. Zgierski, and D. M. Whitfield, "Exploring the mechanism of neighboring group assisted glycosylation reactions," J. Am. Chem. Soc. **120**(51), 13291–13295 (1998).

[30] M. Huang, G. E. Garrett, N. Birlirakis, L. Bohé, D. A. Pratt, and D. Crich, "Dissecting the mechanisms of a class of chemical glycosylation using primary ^{13}C kinetic isotope effects," Nat. Chem. **4**(8), 663–667 (2012).

[31] T. Hosoya, P. Kosma, and T. Rosenau, "Contact ion pairs and solvent-separated ion pairs from D-mannopyranosyl and D-glucopyranosyl triflates," Carbohydr. Res. **401**, 127–131 (2015).

[32] H. Elferink, W. A. Remmerswaal, K. J. Houthuijs, O. Jansen, T. Hansen, A. M. Rijs, G. Berden, J. Martens, J. Oomens, J. D. C. Codée, and T. J. Boltje, "Competing C-4 and C-5-acyl stabilization of uronic acid glycosyl cations," Chem.: Eur. J. **28**(63), e202201724 (2022).

[33] W. A. Remmerswaal, T. de Jong, K. N. A. van de Vrande, R. Louwersheimer, T. Verwaal, D. V. Filippov, J. D. C. Codée, and T. Hansen, "Backside versus frontside S_N2 reactions of alkyl triflates and alcohols," Chem.: Eur. J. **30**(25), e202400590 (2024).

[34] A. Laio and M. Parrinello, "Escaping free-energy minima," Proc. Natl. Acad. Sci. U. S. A. **99**(20), 12562–12566 (2002).

[35] T.-R. Li, F. Huck, G. Piccini, and K. Tiefenbacher, "Mimicry of the proton wire mechanism of enzymes inside a supramolecular capsule enables β-selective *O*-glycosylations," Nat. Chem. **14**(9), 985–994 (2022).

[36] T.-R. Li, G. Piccini, and K. Tiefenbacher, "Supramolecular capsule-catalyzed highly β-selective furanosylation independent of the S_N1/S_N2 reaction pathway," J. Am. Chem. Soc. **145**(7), 4294–4303 (2023).

[37] Y. Fu, L. Bernasconi, and P. Liu, "*Ab initio* molecular dynamics simulations of the S_N1/S_N2 mechanistic continuum in glycosylation reactions," J. Am. Chem. Soc. **143**(3), 1577–1589 (2021).

[38] S. Grimme, C. Bannwarth, and P. Shushkov, "A robust and accurate tight-binding quantum chemical method for structures, vibrational frequencies, and noncovalent interactions of large molecular systems parametrized for all

spd-block elements (Z = 1–86)," J. Chem. Theory Comput. **13**(5), 1989–2009 (2017).
[39]S. van der Vorm, T. Hansen, H. S. Overkleeft, G. A. van der Marel, and J. D. C. Codée, "The influence of acceptor nucleophilicity on the glycosylation reaction mechanism," Chem. Sci. **8**(3), 1867–1875 (2016).
[40]S. van der Vorm, H. S. Overkleeft, G. A. van der Marel, and J. D. C. Codée, "Stereoselectivity of conformationally restricted glucosazide donors," J. Org. Chem. **82**(9), 4793–4811 (2017).
[41]P. Raiteri, A. Laio, F. L. Gervasio, C. Micheletti, and M. Parrinello, "Efficient reconstruction of complex free energy landscapes by multiple walkers metadynamics," J. Phys. Chem. B **110**(8), 3533–3539 (2006).
[42]A. Barducci, G. Bussi, and M. Parrinello, "Well-tempered metadynamics: A smoothly converging and tunable free-energy method," Phys. Rev. Lett. **100**(2), 020603 (2008).
[43]T. D. Kühne, M. Iannuzzi, M. Del Ben, V. V. Rybkin, P. Seewald, F. Stein, T. Laino, R. Z. Khaliullin, O. Schütt, F. Schiffmann, D. Golze, J. Wilhelm, S. Chulkov, M. H. Bani-Hashemian, V. Weber, U. Borštnik, M. Taillefumier, A. S. Jakobovits, A. Lazzaro, H. Pabst, T. Müller, R. Schade, M. Guidon, S. Andermatt, N. Holmberg, G. K. Schenter, A. Hehn, A. Bussy, F. Belleflamme, G. Tabacchi, A. Glöß, M. Lass, I. Bethune, C. J. Mundy, C. Plessl, M. Watkins, J. VandeVondele, M. Krack, and J. Hutter, "CP2K: An electronic structure and molecular dynamics software package—Quickstep: Efficient and accurate electronic structure calculations," J. Chem. Phys. **152**(19), 194103 (2020).
[44]J. VandeVondele, M. Krack, F. Mohamed, M. Parrinello, T. Chassaing, and J. Hutter, "QUICKSTEP: Fast and accurate density functional calculations using a mixed Gaussian and plane waves approach," Comput. Phys. Commun. **167**(2), 103–128 (2005).
[45]G. Bussi, D. Donadio, and M. Parrinello, "Canonical sampling through velocity rescaling," J. Chem. Phys. **126**(1), 014101 (2007).
[46]G. A. Tribello, M. Bonomi, D. Branduardi, C. Camilloni, and G. Bussi, "PLUMED 2: New feathers for an old bird," Comput. Phys. Commun. **185**(2), 604–613 (2014).
[47]M. Sagiroglugil, Q. Liao, A. Planas, and C. Rovira, "Formation of a covalent adduct in retaining β-Kdo glycosyl-transferase WbbB via substrate-mediated proton relay," ChemCatChem **16**(20), e202400769 (2024).
[48]J. D. C. Codée, R. E. J. N. Litjens, R. den Heeten, H. S. Overkleeft, J. H. van Boom, and G. A. van der Marel, "Ph_2SO/Tf_2O: A powerful promotor system in chemoselective glycosylations using thioglycosides," Org. Lett. **5**(9), 1519–1522 (2003).
[49]G. Piccini and M. Parrinello, "Accurate quantum chemical free energies at affordable cost," J. Phys. Chem. Lett. **10**(13), 3727–3731 (2019).
[50]L. Bonati, V. Rizzi, and M. Parrinello, "Data-driven collective variables for enhanced sampling," J. Phys. Chem. Lett. **11**(8), 2998–3004 (2020).
[51]E. Trizio and M. Parrinello, "From enhanced sampling to reaction profiles," J. Phys. Chem. Lett. **12**(35), 8621–8626 (2021).
[52]P. Kang, E. Trizio, and M. Parrinello, "Computing the committor with the committor to study the transition state ensemble," Nat. Comput. Sci. **4**(6), 451–460 (2024).
[53]E. Trizio, P. Kang, and M. Parrinello, "Everything everywhere all at once: A probability-based enhanced sampling approach to rare events," Nat. Comput. Sci. **5**, 582–591 (2025).
[54]R. David, M. de la Puente, A. Gomez, O. Anton, G. Stirnemann, and D. Laage, "ArcaNN: Automated enhanced sampling generation of training sets for chemically reactive machine learning interatomic potentials," Digital Discovery **4**, 54–72 (2025).
[55]S. Vandenhaute, M. Cools-Ceuppens, S. DeKeyser, T. Verstraelen, and V. Van Speybroeck, "Machine learning potentials for metal-organic frameworks using an incremental learning approach," npj Comput. Mater. **9**(1), 19 (2023).
[56]J. Vandermause, S. B. Torrisi, S. Batzner, Y. Xie, L. Sun, A. M. Kolpak, and B. Kozinsky, "On-the-fly active learning of interpretable Bayesian force fields for atomistic rare events," npj Comput. Mater. **6**(1), 20 (2020).
[57]S. Perego and L. Bonati, "Data efficient machine learning potentials for modeling catalytic reactivity via active learning and enhanced sampling," npj Comput. Mater. **10**(1), 291 (2024).